A Novel Technique for Manufacturing Metal-Bonded Nd-Fe-B Magnets by Squeeze Casting

JUN-FA JI and CHUEN-GUANG CHAO

A new method was developed for forming Nd-Fe-B rapidly quenched ribbon to metal-bonded magnets. The process was carried out by a squeeze casting technique. The A356 aluminum alloy and zinc alloy (ZAS) were used as metal binders. The energy product (BH) of A356-bonded magnet was 62.2 k J/m^3 and that of ZAS-bonded magnet was 61.2 k J/m^3. The maximum bending strength of ZAS-bonded magnets (259 MPa) was greater than that of A356-bonded magnets (148 MPa). The corrosion behavior of both magnets was studied in the salt spray test and the magnetization flux loss was measured. The magnetization flux loss of ZAS-bonded magnets is less than that of A356-bonded magnets due to Zn as a sacrificial anode to protect MQ powders.

I. INTRODUCTION

SINTERED rare-earth permanent magnets (REPMs) such as $SmCo_5$, $Sm_2 TM_{17}$, and Nd-Fe-B offer high-energy density and resistance to demagnetization but they are expensive, especially if their full range of properties is not required (as is often the case in electrical machines).[1–4] There are many industrial applications of REPMs due to previously mentioned properties. However, REPMs have some practical shortcomings: they are hard and brittle, difficult to produce in thin or intricate shapes, and large section sizes are nonuniform in their properties. Many of these disadvantages can be eliminated by bonded magnets, which are mainly composed of magnet powders and binder materials. There are many variations of bonded magnets according to the combination of powder and binder.[5–12] Rubbers, elastomers, polymers, and low melting point metal and alloys can be used as the binder. Bonded magnets are less expensive and easier to produce, especially in the case of complex-shape parts. Polymer bonded magnets are very useful near room temperature but deteriorate in air at elevated temperatures. Even at the specified maximum use limits, between about +60 °C and +125 °C, the rate of loss of coercivity and remanence is often intolerable. Thermal cycling can also have disastrous consequences.[6,12] Compared to thermal conductivity of polymer-bonded magnet, the high thermal conductivity of metal-matrix permanent magnets allows for easy heat removal (important for many electrical machines and microwave tubes) and would facilitate temperature uniformity in critical applications such as nuclear magnetic resonance (NMR) CAT-scanner magnets. The combination of high thermal conductivity and the ability to dilute the magnetic flux to specified values has already been used to successfully make two prototype traveling wave tube stacks for the United States army.[13] Suzuki[5] reported that zinc-bonded magnets were prepared from the powder by a compression molding process. Strnat et al.[6] used lead-tin solder as a binder. Rodewald et al.[10] reported that the remanent polarization

and the coercivity of the magnet with 5 wt pct Zn additions were 0.66 T and 880 kA/m, respectively. Rowlinson et al.[14] used a rotary forging technique to fabricate soft metal (Al, Zn, Sn, and Cu) bonded Nd-Fe-B magnets. However, most of the reports used powder metallurgical techniques and rotary forging to produce metal-bonded magnets, which were relatively high cost components due to the variety of processing steps employed. Several studies employed squeeze casting to produce metal matrix composites.[15,16] Squeeze casting is a method that applies pressure to force molten alloys into preforms made of ceramic particles. Preforms can be manufactured by a number of known ceramic-processing routes, including injection molding, dry pressing, and slip casting.

The discovery of Nd-Fe-B permanent magnet materials in 1983 had kindled technological and scientific interest.[17,18,19] Unfortunately, Nd-Fe-B is highly vulnerable to corrosive attack and their large-scale commercial applications are hindered partly by this drawback. To improve the corrosion resistance of these magnets, methods such as doping and surface coating with Al, Zn, Cr, or Ni have been employed.[20–23] In this current work, we manufactured the metal-bonded (Al alloy and Zn alloy) Nd-Fe-B magnets by squeeze casting. We also investigated the magnetic, mechanical, and corrosion properties of the metal-bonded magnets.

II. EXPERIMENTAL

Rapidly solidified Nd-Fe-B alloys (MQ-B) were produced by the Magnequench Division of GM Corporation (Anderson, IN). The MQ-B powders of different plate sizes were used in the present experiment. The original powder was sieved to obtain three levels of the length—fine plates (37 to 105 μm), medium plates (106 to 150 μm), and coarse plates (>188 μm). The characteristics of MQ-B powder are listed in Table I. The matrix alloys were aluminum alloy

JUN-FA JI, Process Engineer, is with the Wafer Test Factory, Philips Semiconductor, Kaohsiung, Taiwan 811, Republic of China. CHUEN-GUANG CHAO, Professor, is with the Department of Materials Science and Engineering, National Chiao Tung University, Hsinchu, Taiwan 300, Republic of China.

Table I. Magnetic Characteristics of MQ Powder

Residual induction (Br)	0.83 T
Intrinsic coercivity (Hci)	7.8×10^5 A/m
Energy product (BH)$_{max}$	104 kJ/m^3
Temperature coefficient of Br to 100 °C	−0.105 pct C
Maximum operating temperature	110 °C

Table II. Chemical Composition of MQ Powder, A356, and ZAS Alloys

Compound (Wt Pct)	Fe	Nd	B	Co	Cu	Mg	Mn	Si	Zn	Ti	Al	Pb
MQ	66.8	24	0.98	4.8	—	—	—	—	—	—	—	—
A356	0.20	—	—	—	0.20	0.25 to 0.45	0.1	6.5 to 7.5	0.10	0.20	bal	—
ZAS	<0.08	—	—	—	3.11	0.036	—	—	bal	—	3.92	<0.01
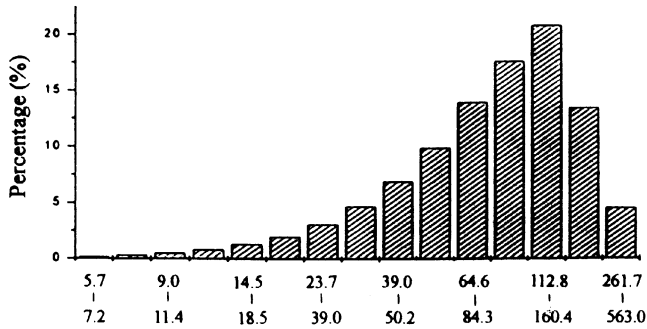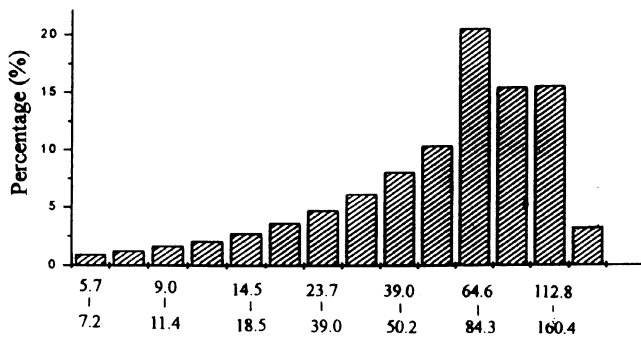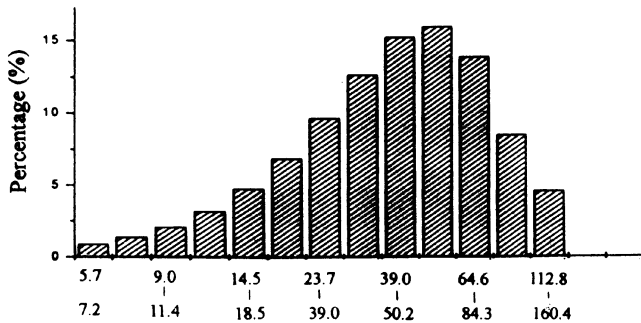
Fig. 1—The sieved MQ powders of three levels; the size distribution for (*a*) coarse (*b*) medium, and (*c*) fine powder measured after the compaction process of the preform.

Fig. 2—Optical microstructure of ZAS-bonded magnets made from (*a*) coarse (*b*) medium, and (*c*) fine MQ powder.

(A356) and zinc alloy (ZAS). The chemical compositions of MQ-B, A356, and ZAS are listed in Table II. The metal-bonded magnets were fabricated by squeeze casting. The experiments included two parts: part I was the same volume fraction of MQ powders with various plate sizes; and part II was the same plate size with different volume fractions. One hundred grams of MQ-B powders were placed into a 5 × 5 cm square mold and compacted by hydraulic pressure. The compacting pressure was 95 MPa for fine powders, 48 MPa for medium powders, and 35 MPa for coarse powders in order to obtain the same height of the preform. Because the fine powders were difficult to pack layer on layer, a higher pressure was required to obtain the same height of the preform. In order to understand if the MQ powders were broken during the compaction process, a laser particle size analyzer was used to measure the plate size distribution. In addition, we chose the compaction pressures 95, 65, and 35 MPa, respectively, for coarse MQ-B powders in order to obtain the various heights of preforms, which had different volume fractions of MQ powders. The preform was pre-heated to 180 °C and then placed into the mold. The mold was preheated to 280 °C for Zn and 300 °C for Al. The
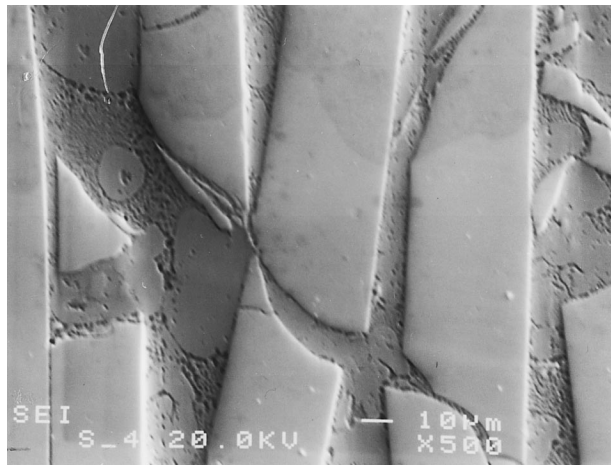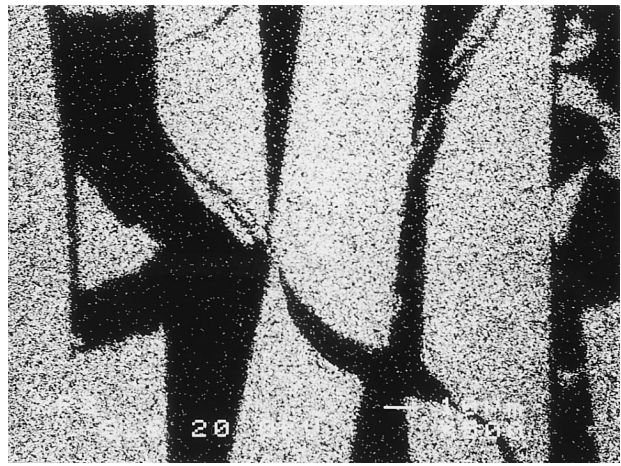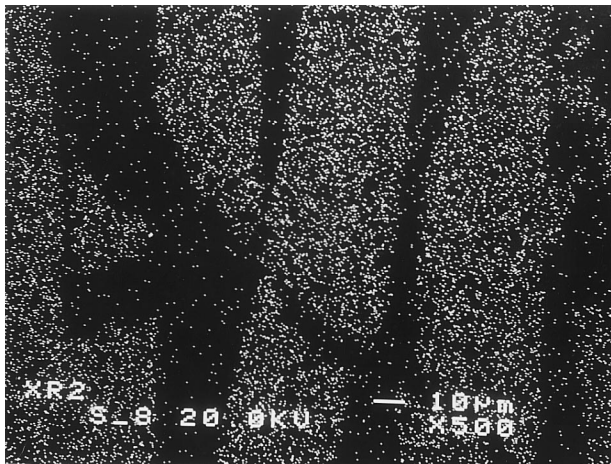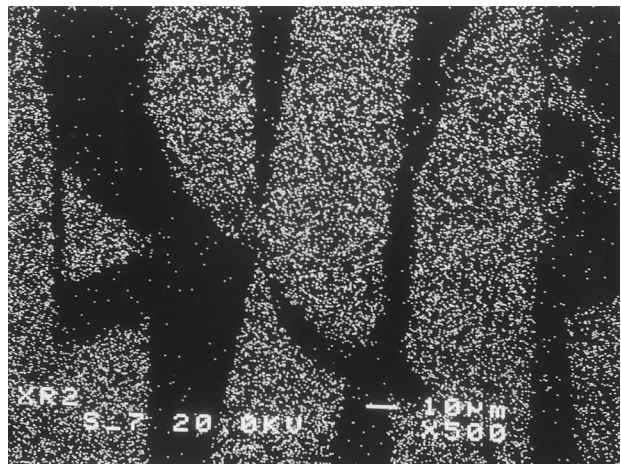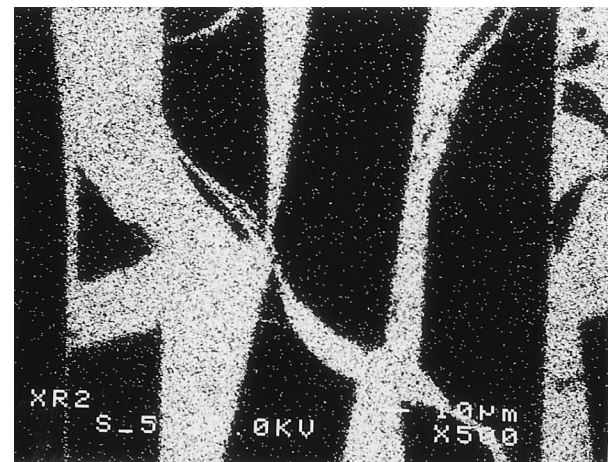
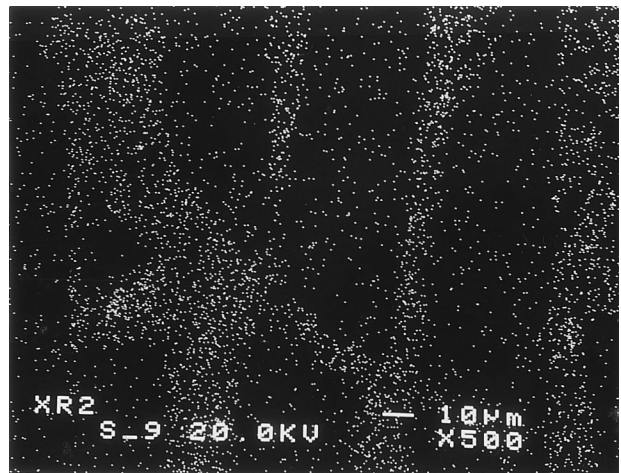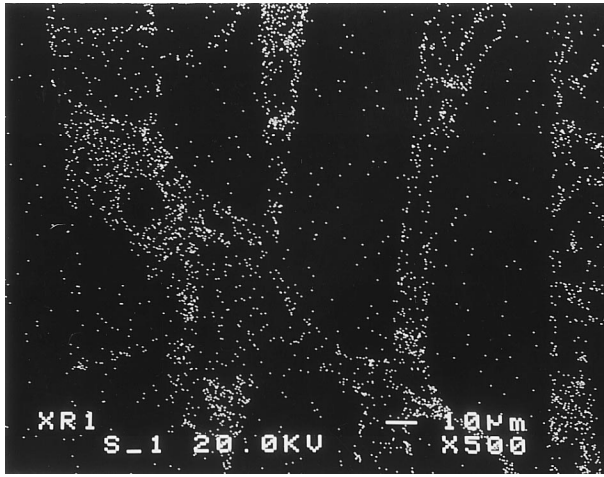Fig. 3—EPMA of ZAS-bonded magnet with coarse powders as squeezed showing (*a*) the electron image of a region and the corresponding X-ray images of (*b*) Fe, (*c*) Nd, (*d*) Co, (*e*) Zn, (*f*) Al, and (*g*) Cu.

liquid metal Al and Zn alloys, at 730 °C and 650 °C, respectively, were squeezed into the same mold as used for compaction with a 40 MPa applied pressure and a holding time of 90 seconds.

Light microscopy was used to observe the microstructure.

Scanning electron microscopy (SEM) was used to examine the morphology, and electron probe micro-analyzer (EPMA) was carried out to identify the phase compositions. The magnetic properties of bonded magnets were measured by a Magnet-Physik Permagraph C magnetometer. According
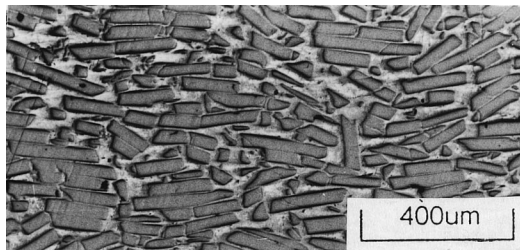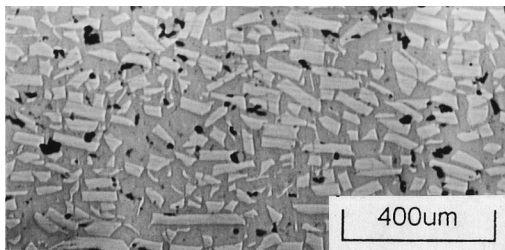
(g)

Fig. 3—Continued. EPMA of ZAS-bonded magnet with coarse powders as squeezed showing (a) the electron image of a region and the corresponding X-ray images of (b) Fe, (c) Nd, (d) Co, (e) Zn, (f) Al, and (g) Cu.
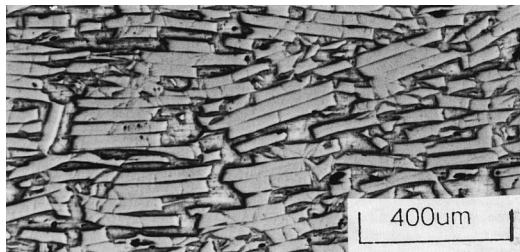
(a)

(b)

(c)

Fig. 4—Optical microstructure of A356-bonded magnets made from (a) coarse, (b) medium, and (c) fine MQ powder.

to the JIS R1601 specification, the three-point bend test was employed to measure the strength of the metal-bonded magnets. The test machine was an Instron 8501 with a 0.5 mm/min compression rate to measure the bending strength.

For each condition, we took eight specimens to obtain the average value. The bending strength (σ_b) is

$$\sigma_b = 3 \times P \times L/2 \times W \times t^2$$

where L is length, W is width, P is load, and t is thickness.

The corrosion behavior was investigated by the normal salt spray test according to the ASTM B117 and G1-90 practices, respectively, using a standard salt spray chamber. The specimens were $25 \times 15 \times 2.2$ mm. After the corrosion test for the specified periods, visual observation of the surface changes and SEM imaging of the sectioned corroded surface were carried out. The weight loss of the corrosive magnets that were cleaned by supersonic cleaner was calculated and it was plotted against exposure time. Then, the samples of the corrosive magnets were redetermined by Gauss meter to measure the open circuit of remanent flux density.

III. RESULTS

A. Microstructure

Figure 1 shows the plate size distribution for coarse, medium, and fine MQ powders by the compaction process. The results show that the length of plates slightly decreases during the compaction procedure. Figure 2 illustrates the typical photomicrographs of the ZAS-bonded magnets, showing a homogeneous distribution of plates and less than 1 vol pct porosity. The results of typical EPMA of a coarse powder ZAS-bonded magnet are shown in Figure 3. The secondary electron image of the microstructure of magnets, the MQ powder in the ZAS matrix, is shown in Figure 3(a). Figures 3(b) through (g) indicate the corresponding X-ray images of Fe, Nd, Co, Zn, Al, and Cu, respectively. No obvious reaction is found between the ZAS alloy and MQ powder. Figure 4 provides the photomicrographs of the A356-bonded magnets, showing a homogeneous distribution of plates. The coarse and medium plate specimens have less than 1 vol pct porosity, but the fine plate specimen has about 6 vol pct porosity. The secondary electron image of the microstructure of magnets, the coarse MQ powder in A356 matrix, is shown in Figure 5(a). Figures 5(b) through (f) indicate the corresponding X-ray images of Fe, Nd, Co, Al, and Si, respectively. There is obvious chemical reaction between A356 alloy and MQ powder.

B. Magnetic Properties

Figure 6 shows the influence of compaction pressure on magnetic properties of metal-bonded magnets for the coarse powder specimens. Observed characteristics of the metal-bonded magnets are as follows: the maximum remanence Br = 0.611 T, and the energy product $(BH)_{max}$ = 62.2 kJ/m^3 for ZAS-bonded magnet; and Br = 0.59 T, and $(BH)_{max}$ = 61.2 kJ/m^3 for A356-bonded magnet. The remanent magnetization (Br) and $(BH)_{max}$ increase with increasing compaction pressure in both ZAS-bonded and A356-bonded magnets. Figure 7 shows that the $(BH)_{max}$ of A356-bonded magnets is higher than that of ZAS-bonded magnets at the same Br. The demagnetization curves of coarse powder metal-bonded magnets are plotted in Figure 8. The saturation magnetization is almost the same at the value of 1.19×10^6
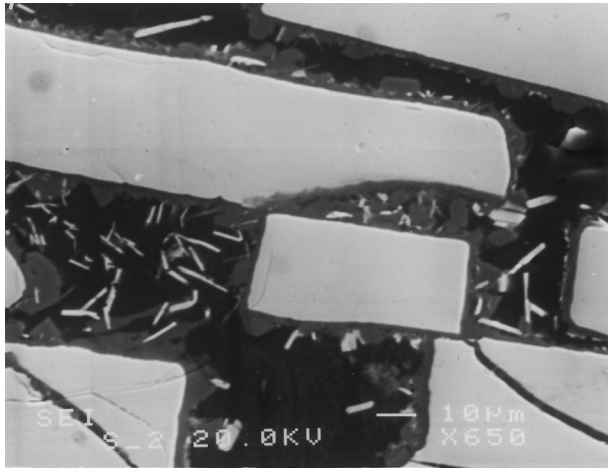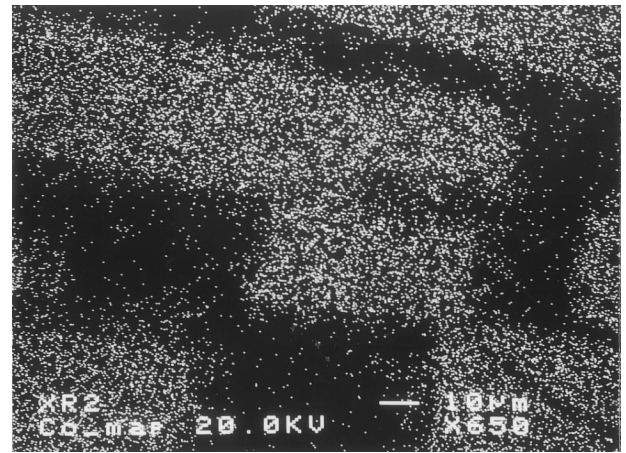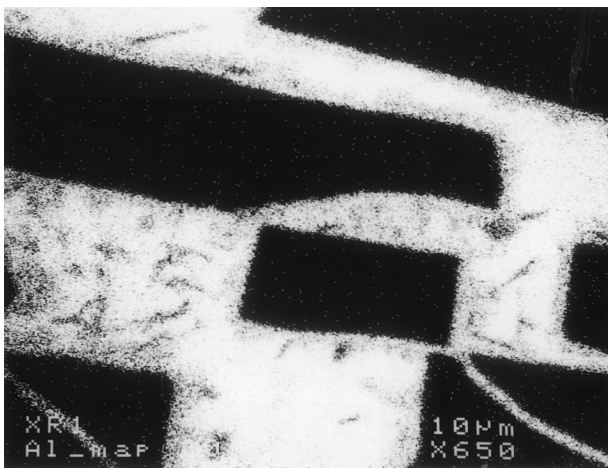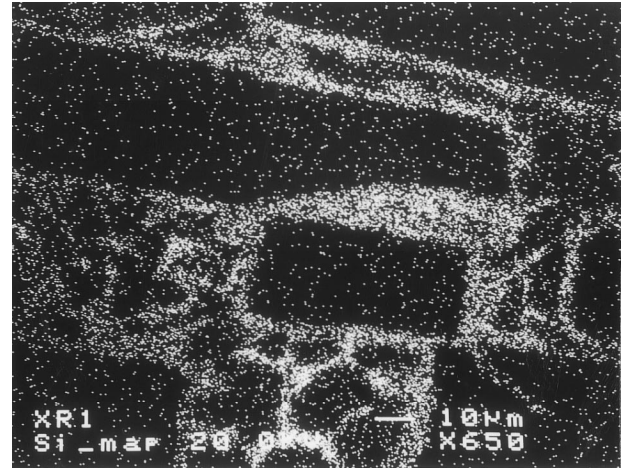
(a)
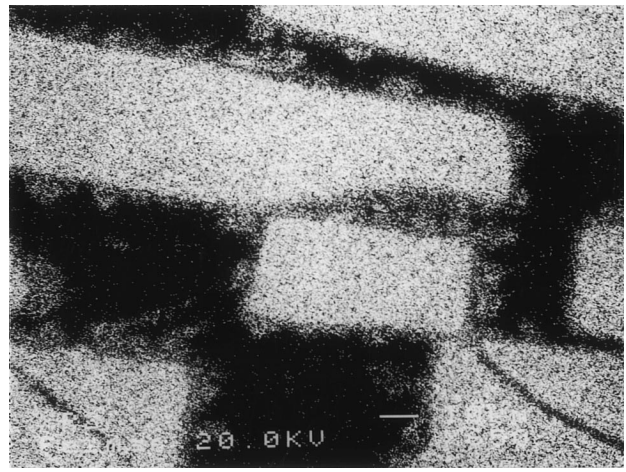
(b)
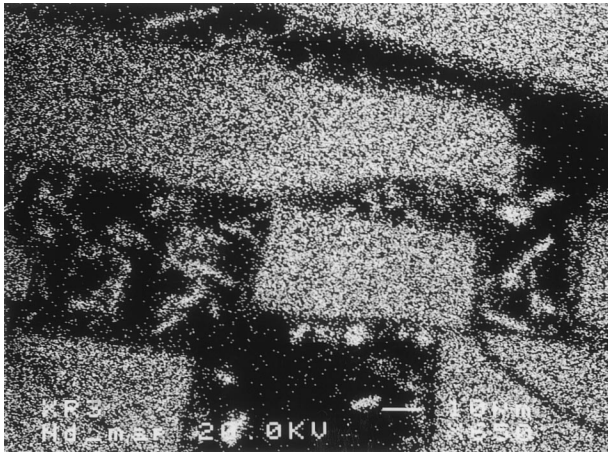
(c)

(d)

(e)

(f)

Fig. 5—EPMA of A356-bonded magnet with coarse powders as-squeezed, showing (a) the electron image of a region and the corresponding X-ray images of (b) Fe, (c) Nd, (d) Co, (e) Al, and (f) Si.

A/m. The remanence (Br) is 0.552 and 0.54 T for A356-bonded and ZAS-bonded magnets, respectively. The intrinsic coercivity (Hci) is 7.72×10^5 and 7.59×10^5 for A356-bonded and ZAS-bonded magnets, respectively.

C. Bending Strength

The bending strengths of metal-bonded magnets are listed in Table III. The maximum bending strength is about 259
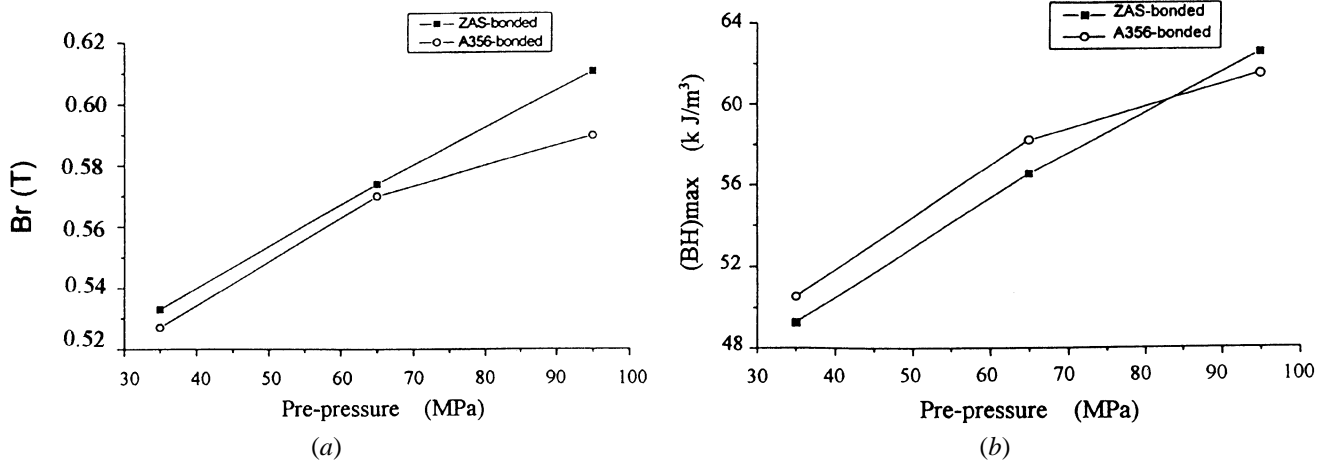
Fig. 6—The relationship between compaction pressure and (*a*) Br and (*b*) $(BH)_{max}$ for coarse powder specimens.
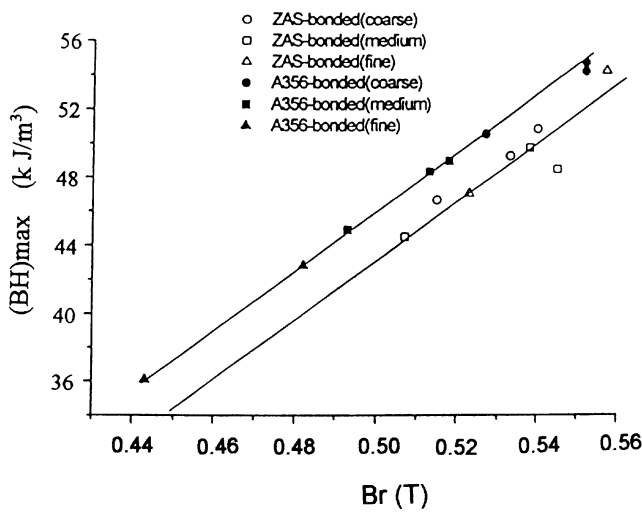

Fig. 7—The relationship between $(BH)_{max}$ and Br of ZAS-bonded and A356-bonded magnets.
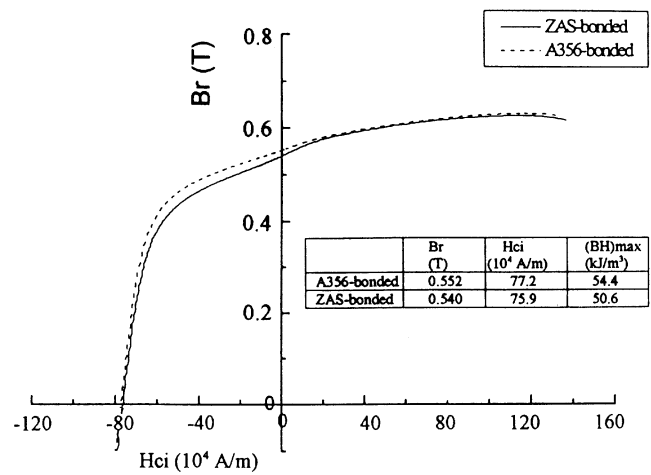
Fig. 8—The demagnetization curves of ZAS-bonded and A356-bonded magnets with coarse powders.

Table III. The Bending Strength of the Metal-Bonded Magnets

Strength	Materials			
	A356	A356-Bonded Magnet (Coarse)	A356-Bonded Magnet (Medium)	A356-Bonded Magnet (Fine)
Bending strength (MPa)	364 ± 3	148 ± 4	126 ± 2	105 ± 6
Percentage	100 pct	41 pct	35 pct	29 pct
	Materials			
	ZAS	ZAS-Bonded Magnet (Coarse)	ZAS-Bonded Magnet (Medium)	ZAS-Bonded Magnet (Fine)
Bending strength (MPa)	431 ± 2	252 ± 5	257 ± 3	259 ± 2
Percentage	100 pct	58 pct	60 pct	63 pct

and 148 MPa for ZAS-bonded and A356-bonded magnets, respectively. The bending strength of ZAS-bonded magnets is about 63 pct of that of ZAS alloy (431 MPa), while the bending strength of A356-bonded magnets is only about 41 pct of that of A356 alloy (364 MPa). In addition, all the specimens have almost the same bending strength for ZAS-bonded magnets, but the coarse plate specimens have the maximum bending strength for A356-bonded magnets.

D. *Corrosion Behavior*

Figure 9 exhibits the weight loss of magnetized metal-bonded magnets in an aerated salt chamber as a function of time. The weight loss increases rapidly in the first 4 days. Then, it slightly increases after that. The weight loss of ZAS-bonded magnets is higher than that of A356-bonded magnets. The magnetization flux loss of the metal-bonded magnets
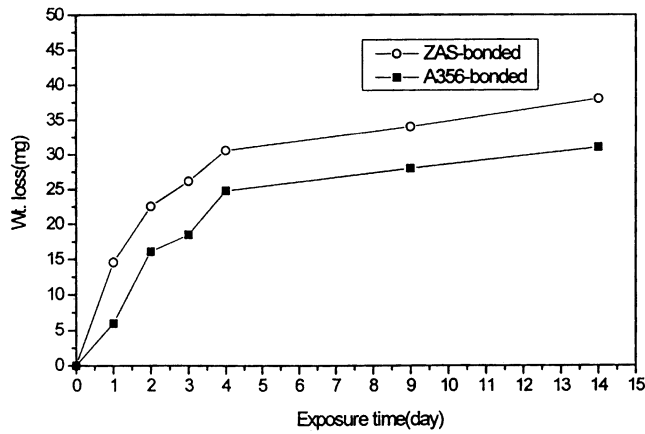
Fig. 9—The weight loss of metal-bonded magnets with coarse powders in the salt spray test.
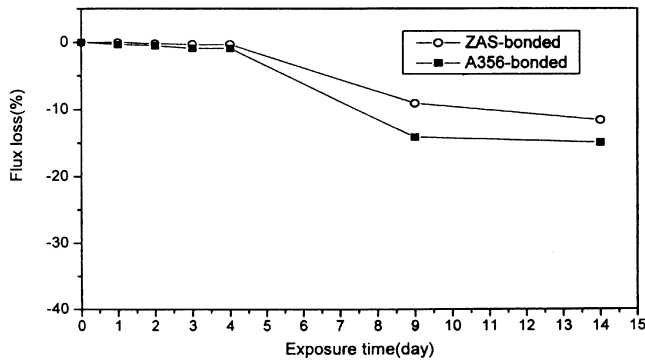

Fig. 10—The permanent flux loss of metal-bonded magnets with coarse powders in the salt spray test.
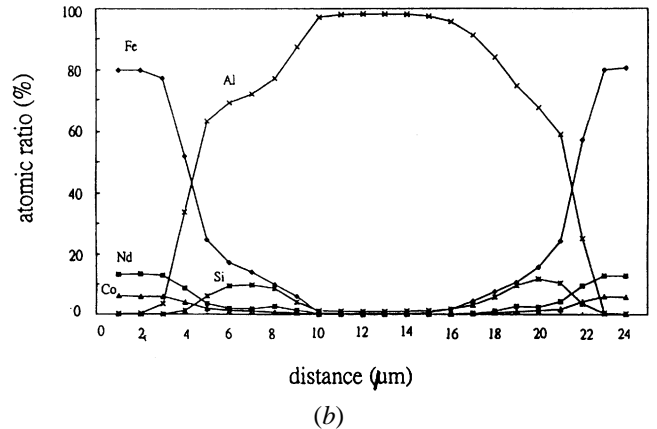

(a)

(b)

Fig. 11—Profile of atomic diffusion in (a) ZAS-bonded and (b) A356-bonded magnets with coarse powders.

is almost the same in the first 4 days and, afterward, it increases with increasing exposure time. After 14 days, the magnetization flux loss is 9.1 and 14.1 pct for ZAS-bonded magnets and A356-bonded magnets, respectively, as shown in Figure 10.

IV. DISCUSSIONS

There is no obvious interfacial reaction in Zn-bonded magnets but an apparent reaction in A356-bonded magnets, as shown in Figures 3 and 5. Figure 11 illustrates the profile of atomic diffusion in metal-bonded magnet. The diffusion layer, which includes Zn, Nd, and Fe, is about 2 μm in the ZAS-bonded magnet in Fig. 11(a). However, the diffusion layer of A356-bonded magnet illustrated in Figure 11(b), which includes Al, Fe, Nd, Co, and Si, reaches 7 μm.

Figure 7 shows that the $(BH)_{max}$ decreases with decreasing MQ powder size in A356-bonded magnet but is independent of MQ powder size in ZAS-bonded magnet. The reason is that there is no obvious interfacial reaction in ZAS-bonded magnets but an apparent reaction in A356-bonded magnets. The more interfaces of matrix and MQ powders there are, the more reaction phases are produced. The fine powder specimens have more interfaces with the same volume fraction of MQ powders. Therefore, $(BH)_{max}$ decreases with decreasing powder size by production of nonmagnetic phases. However, the $(BH)_{max}$ of ZAS-bonded magnets is
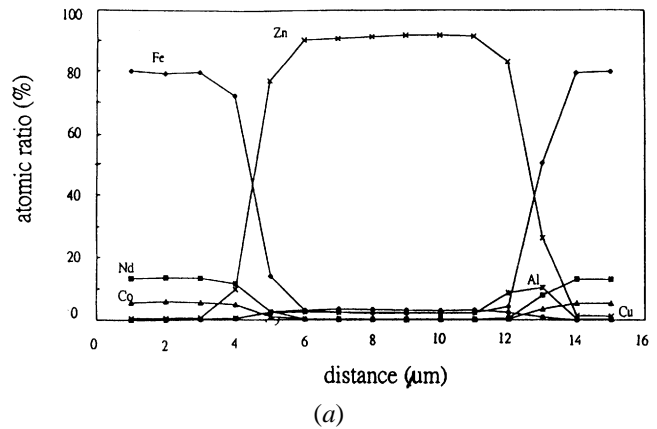
independent of the powder size due to the lack of reaction in the ZAS-bonded magnet. Figure 8 shows the demagnetization curve of the two magnetic composites. The respective demagnetization behavior of the two magnetic composites is about the same. Thus, the demagnetization properties of the metal-bonded magnets are independent of the binder.

Figures 12 and 13 show the fracture surfaces of ZAS-bonded magnets and A356-bonded magnets, respectively. The fracture surfaces of the two magnetic composites display a typical fracture surface of metallic glasses. The longest flaw in the MQ powder dictates the bending strength of magnetic composite, and the probability of finding longer defects increases with the powder size. Thus, coarse powder fails more easily than does fine powder. Therefore, the bending strength of ZAS-bonded magnet slightly increases with decreasing MQ powder size, as shown in Table III. However, the bending strength of A356-bonded magnet decreases with decreasing MQ powder size. One reason is due to the fine powder specimen of 6 vol. pct porosity shown in Fig. 4(c). The other reason is that the finer powders are much more prone to produce brittle phase ($Al_{13}Fe_4$, $FeAl_2$, and $Nd_2Fe_{15}Al_2$). It is obvious that the interface of matrix and MQ powder affects the magnetic and mechanical properties of metal-bonded magnets.
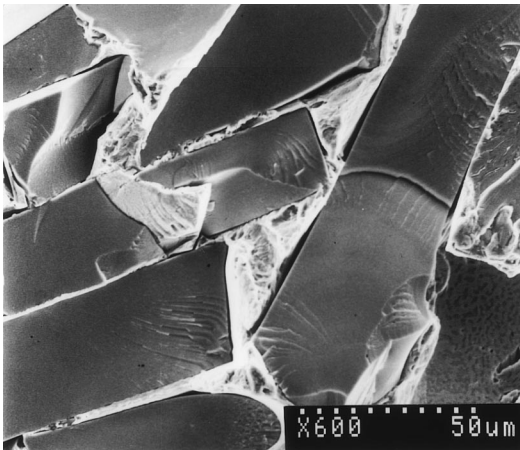
Figure 6 shows that Br and $(BH)_{max}$ increase with increasing compaction pressure for the coarse powder specimens. The smaller compaction pressure results in the lower volume fraction of MQ powder in metal-bonded magnets. Large
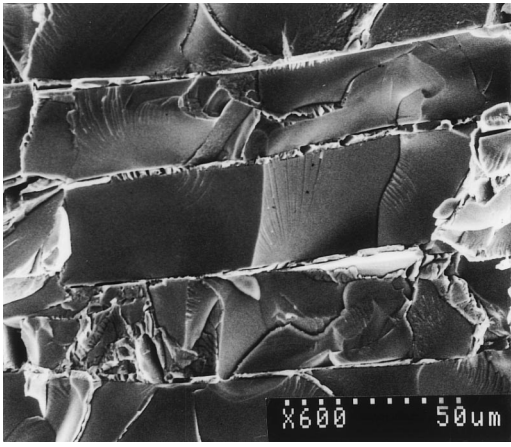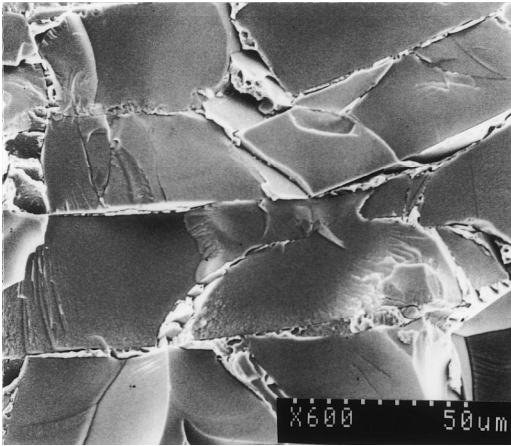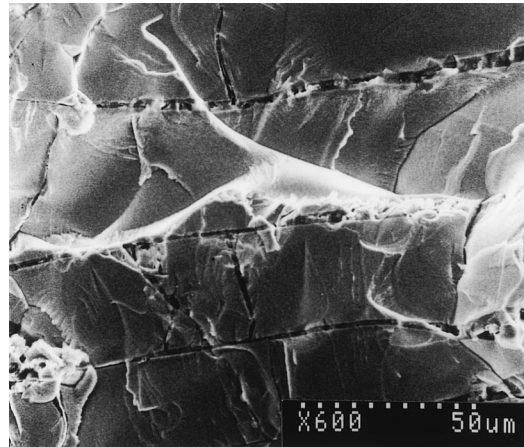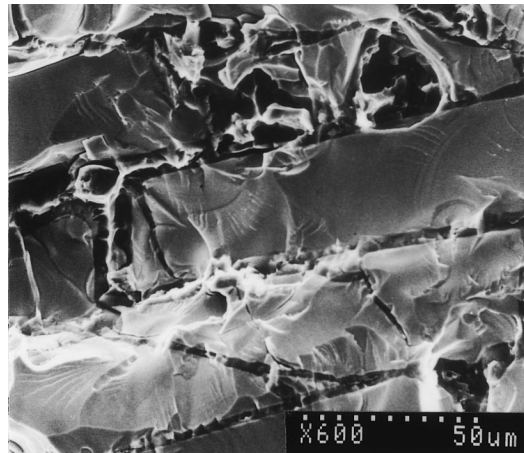
Fig. 12—Fracture surface of ZAS-bonded magnets for bending specimens: (*a*) coarse, (*b*) medium, and (*c*) fine MQ powder.

Fig. 13—Fracture surface of A356-bonded magnets for bending specimens: (*a*) coarse, (*b*) medium, and (*c*) fine MQ powder.

amounts of binder (A356 or ZAS) result in significant dilution of the magnetic properties with Br (0.83T) and $(BH)_{max}$ (104 k J/m^3) for no binder.
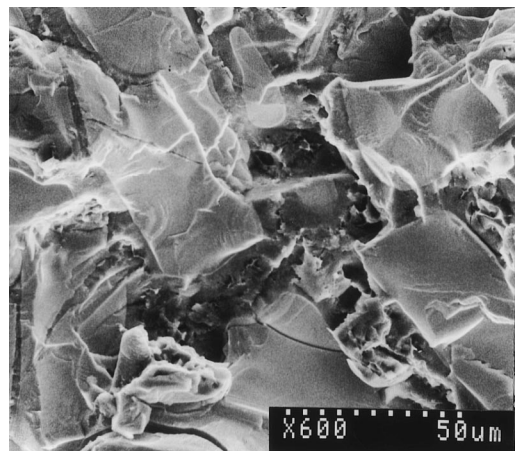
Man *et al.*[24] reported that a layer of brown rust (*e.g.*, hydrated Fe_3O_4) was uniformly distributed over a bare NdFeB specimen surface after 1 hour of exposure. This was due to the high iron content that was oxidized rapidly in the salt spray environment. In our study, white rust was observed on the surface of the ZAS-bonded magnet and brown rust was observed on the surface of the A356-bonded magnet shown in Figure 14(b). This white corrosion product of zinc is hydrated zinc oxide. It is apparent that zinc is a sacrificial anode. However, for the A356-bonded magnet, brown rust was formed due to the corrosion of MQ powders. Figure 15 also illustrates the corroded surface of ZAS-bonded and
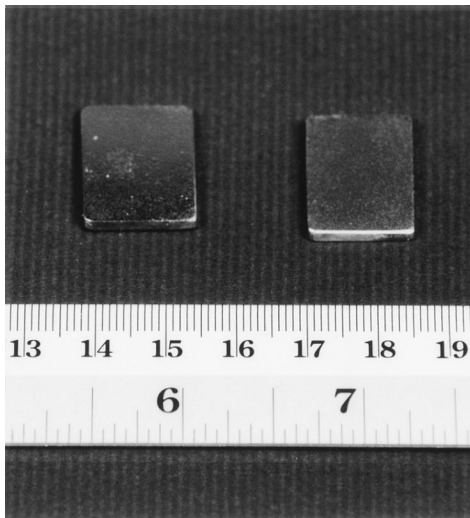
(a)

(b)

Fig. 14—Specimens of the metal-bonded magnets (a) before and (b) after salt spray test for 2 weeks. Specimens on the left are ZAS-bonded magnet, and those on the right are A356-bonded magnet.
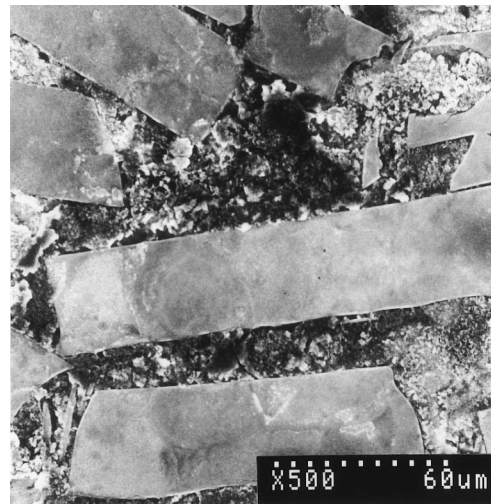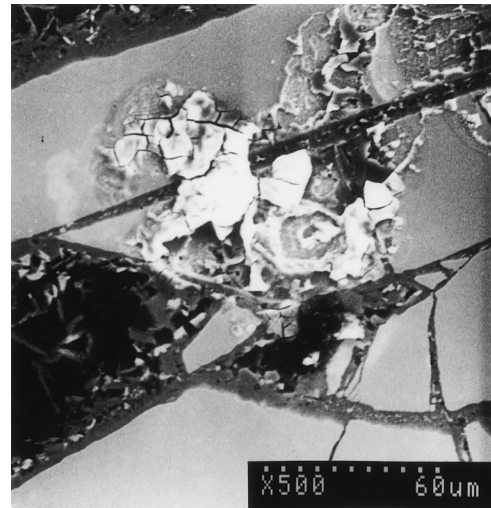

(a)

(b)

Fig. 15—Comparison of the corroded surface of (a) ZAS-bonded and (b) A356-bonded magnets after 1 day corrosion test.

A356-bonded magnets. Figure 15(a) shows that the sacrificial zinc matrix may be capable of reducing the corrosion of MQ powders, but Figure 15(b) shows that the aluminum matrix cannot provide effective protection to the MQ powders. Although aluminum is electrochemically more active than MQ powders, the effect of sacrificial anode is reduced because since the oxide film (Al_2O_3) covers the aluminum matrix. Figure 10 shows that the magnetization flux loss is essentially nil during the initial rapid corrosion rate, but it is rather large when the corrosion rate decreases. It is well known that the larger the corrosion layer is, the smaller the magnetization flux density. It may be presumed that the deterioration of the magnetization flux is proportional to the extent of corrosive reactions from the surface of the magnet shown in Figure 16. In the first 4 days, the magnetization flux loss is essentially nil while the corrosion weight loss rapidly increases. The weight loss was obvious when the supersonic cleaner easily cleaned up the corrosive layer. It may be due to the corrosion occurring on the surface. In the

meantime, the magnetization fluxes are almost the same owing to the corrosive layer removed. However, the magnetization flux loss increases after 4 days because the corrosion depth increases. The weight loss slightly increases because supersonic cleaner cannot remove the internally corrosive parts. In addition, the magnetization flux loss of ZAS-bonded magnets is less than that of A356-bonded magnets due to Zn as a sacrificial anode to protect MQ powders.

V. CONCLUSIONS

The ZAS-bonded magnets and A356-bonded magnets were fabricated by squeeze casting. The results are summarized as follows.

1. The metal-bonded magnets can be easily fabricated by squeeze casting.
2. The maximum energy product $(BH)_{max}$ is 61.2 and 62.2 k J/m^3 for ZAS-bonded magnets and A-356 bonded magnets, respectively.
3. The $(BH)_{max}$ decreases with decreasing MQ powder size

Fig. 16—A schematic representation of the remanent flux density (*a*) before the corrosion test, (*b*) after 4 days corrosion test, and (*c*) after 9 days corrosion test.

in A356-bonded magnets due to apparent interfacial reactions with decreasing powder size.

4. The maximum bending strength of ZAS-bonded magnet (259 MPa) is higher than that of A356-bonded magnet (148 MPa).

5. The magnetization flux loss of ZAS-bonded magnets is less than that of A356-bonded magnets due to Zn as a sacrificial anode to protect MQ powders.

REFERENCES

1. M.Q. Huang, L.Y. Zhang, B.M. Ma, Y. Zheng, J.M. Elbiciki, W.E. Wallace, and S.G. Sankar: *J. Appl. Phys.*, 1991, vol. 70 (10), pp. 6027-29.
2. W. Rodewald, M. Velicescu, B. Wall, and G.M. Reppel: *Proc. 12th Workshop on RE-Magnets and Their Applications*, Canberra, Australia, University West Australia, July, 1992, p. 191.
3. W. Rodewald, B. Wall, M. Kntter, M. Velicescu, and P. Schrey: *37th Annual Conference on Magnetism and Magnetic Materials*, Houston, TX, 1992, p. CP-13.
4. Satoshi Hirosawa and Yoshiyuki Tsubokawa: *J. Magn. Magn. Mater.*, 1990, vol. 84, pp. 309-16.
5. A. Verma, P. Verma, and R.K. Sidhu: *Bull. Mater. Sci.*, 1996, vol. 19(3), pp. 539-548.
6. R.M.W. Strnat, S. Liu, and K.J. Strnat: *Proc. 5th Int. Workshop on Rare Earth Cobalt Permanent Magnets and Their Application*, Roanoke, VA, University of Dayton, June, 1981, pp. 609-28.
7. M. Velicescu, B. Wall, W. Rodewald, and G.M. Reppel: *IEEE Trans.*, 1993, vol. 29 (6), pp. 2827-29.
8. T.S. Chin, K.H. Cheng, and J.M. Yao: *J. Alloys Compounds*, 1995, vol. 222, pp. 148-52.
10. W. Rodewald, B. Wall, M. Kaller, M. Volicescu, and P. Schrey: *J. Appl. Phys.*, 1993, vol. 73 (10), pp. 5899-5901.
11. P.A.P. Wendhansen, A. Handstein, D. Eckert, and K.H. Muller: *Phys. Status Solidi.* 1991, (a), vol. 127, pp. K121-K124.
12. R.M.W. Strnat, S. Liu, and K.J. Strnat: *J. Appl. Phys.*, 1982, vol. 53, p. 2380.
13. R.M.W. Strnat, J.P. Clarke, H.A. Leupoid, and A. Tauber: *J. Appl. Phys.*, 1987, vol. 61 (8), pp. P3463-P3465.
14. N. Rowlinson, M.M.A. Shraf, and I.R. Harris: *J. Magn. Magn. Mater.*, 1989, vol. 80, pp. 93-96.
15. C.R. Cook, D.I. Yun, and W.H. Hunt, Jr.: *Proc. Int. Symp. on Advances in Cast Reinforced Metal Composites*, ASM, Metals Park, OH, 1988, pp. 195-204.
16. S.K. Verma and J.L. Dorcie: *Proc. Int. Symp. on Advances in Cast Reinforced Metal Composites*, ASM, Metals Park, OH, 1988, pp. 115-26.
17. J.F. Herbst: *Rev. Mod. Phys.*, 1991, vol. 63 (4), pp. 819-72.
18. J.F. Herbst, J.J. Croat, and W.B. Yelon: *J. Appl. Phys.*, 1985, vol. 57 (17), pp. 4086-90.
19. V. Panchanathan: *J. Mater. Eng. Performance*, 1995, vol. 4 (4), pp. 423-29.
20. N.C. Ku, C.-D. Qin, C.C. Yu, and D.H.L. Ngs: *IEEE Trans. Magn.*, 1996, vol. 32 (5), pp. 4407-09.
21. C.W. Cheng, H.C. Man, and F.T. Cheng: *IEEE Trans. Magn.*, 1997, vol. 33 (5), 3910-12.
22. T. Minowa, M. Yoshikawa, and M. Honshima: *IEEE Trans. Magn.*, 1998, vol. 25 (5), pp. 3776-78.
23. S.A. Attanasio and R.M. Latanision: *Mater. Sci. Eng. A*, 1995, vol. A198, pp. 25-34.
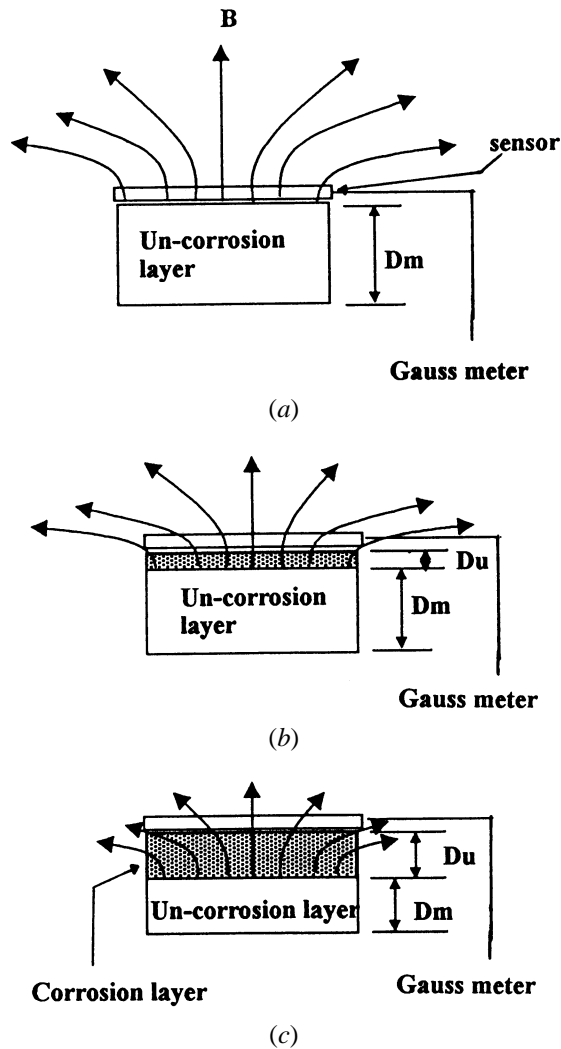24. H.H. Man, H.C. Man, and L.K. Leung: *J. Magn. Mater.*, 1996, vol. 152, pp. 40-46.